ISIJ International, Vol. 32 (1992), No. 3, pp. 316–325

Mathematical Model Coupling Phase Transformations and Temperature Evolutions in Steels

S. DENIS, D. FARIAS and A. SIMON

Laboratoire de Science et Génie des Matériaux Métalliques, Ecole des Mines de Nancy, Parc de Saurupt, 54042 NANCY Cedex, France.

(Received on October 25, 1991; accepted in final form on January 24, 1992)

A mathematical model for calculating phase transformations in steels during rapid heating and cooling is presented. It is based on a rule of additivity. The isothermal kinetics are modelled by Johnson–Mehl–Avrami law. The model describes the kinetics of austenitization during heating, the state of austenite at the end of heating (carbon content, grain size), the kinetics of transformations during cooling, the final microstructure and hardness. The model is worked out firstly on dilatometric specimens without thermal gradients in order to validate the modelling and the input data. Then the application of the model to massive cylinders heated up and cooled down with high thermal gradients is presented.

KEY WORDS: mathematical model; phase transformation; steel, heat treatment.

1. Introduction

In the past a number of studies have dealt with the prediction of microstructural evolutions of steels during cooling. A review has been given in[1,2] to which some other works should be added.[3,4] Only a few studies concern the calculation of the kinetics of austenitization during rapid heating.[4,5] Moreover the modelling of the effect of the state of austenite at the end of heating (inhomogeneous chemical composition, grain size) on the kinetics of phase transformations during cooling has been little taken up. Several authors[4,6,7] have introduced the grain size of austenite as a parameter in the laws describing the isothermal or anisothermal kinetics of transformation. As far as we know only one study[8] takes into account the effect of local carbon content of austenite on the critical cooling rate and on Ms temperature.

Some years ago, we have developed a model for calculating phase transformations during continuous cooling in steels.[1,2]

In this paper we present an extension of this model in order to describe also phase transformations during heating. An approach for taking into account both the effect of the local carbon content of austenite and the effect of the grain size of austenite on the kinetics of phase transformations during cooling is presented. The model is worked out firstly on dilatometric specimens without thermal gradients for which the parameters needed for the validation of the computations are measured.

Then we illustrate how the model works on cylindrical specimens with high thermal gradients. Finally, an application of the model to induction hardening is shown.

2. Description of the Phase Transformation Calculation Model

2.1. Heating

2.1.1. Calculation of Anisothermal Transformation Kinetics

The method used in this paper for calculating phase transformations during continuous heating from isothermal data is based on a rule of additivity. It has been used by several authors[2,5,9] and we recall briefly the principal of the method. The temprature–time curve is discretized in a series of isothermal steps. On each step the volume fraction of new phase formed is calculated by using isothermal transformation kinetics. The isothermal transformation kinetics is modelled according to the law developed by Johnson–Mehl[10] and by Avrami[11]:

$$y_k = y_{\max k}(1-\exp(-b_k t^{nk}))$$

where y_k is the volume fraction of constituent k transformed into austenite ($k=1$ pearlite, $k=2$ ferrite) and b_k and n_k are temperature dependent parameters. At each temperature, the coefficients n_k and b_k are calculated by using two points corresponding to a given percentage of phase formed (10 and 90% for example) obtained from the isothermal kinetics of transformation or from the Isothermal Heating Diagram. $y_{\max k}$ is the maximum volume fraction of austenite that can be formed. The method for quantifying the phase transformations is given on **Fig. 1**, it is the same as the one used previously on cooling.[2]

From the volume fraction of austenite y_i formed up

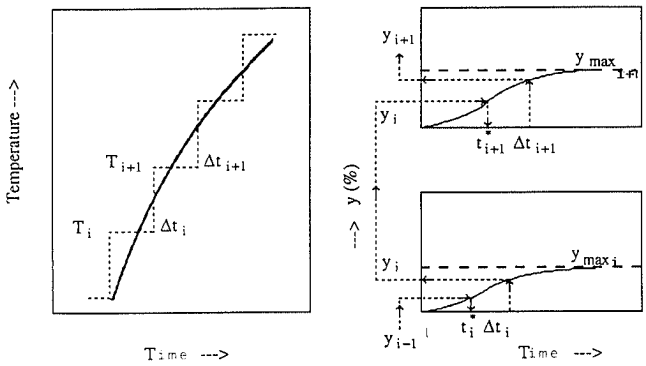

Fig. 1. Schematic representation of the calculation of new phase formed.

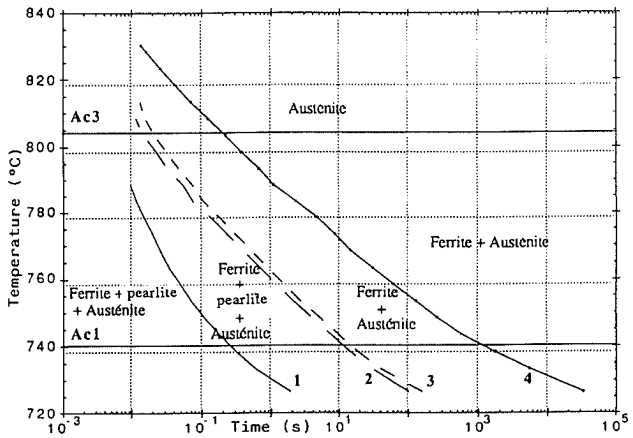

Fig. 2. Isothermal transformation heating diagram for a XC42 carbon steel.

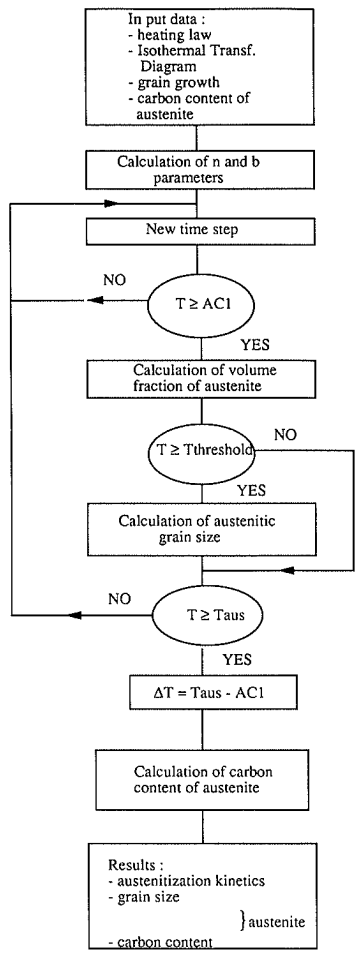

Fig. 3. Flow chart of the phase transformation calculation model on heating.

to the end of time step i, the position on the isothermal kinetics at temperature T_{i+1} is found through the fictitious time t^*_{i+1}:

$$t^*_{i+1}=\frac{\ln\left(1-\dfrac{y_{ki}}{y^{\max}_{k(i+1)}}\right)^{1/n_{i+1}}}{b_{i+1}}$$

The fictitious time is incremented by Δt_{i+1} in order to calculate the volume fraction of austenite at the end of time step $i+1$:

$$y_{k(i+1)}=y^{\max}_{k(i+1)}[1-\exp(-b_{i+1}(t_{i+1}+\Delta t_{i+1})^{n_{i+1}})]$$

An example of an IT heating diagram as it is used in our model for a hypoeutectoïd carbon steel with a ferrite–pearlite microstructure is presented on **Fig. 2**.

The different steps of the transformation from ferrite–pearlite microstructures into austenite, the mechanisms and the kinetics of these transformations have been widely treated and discussed in the literature.[12-17] From the IT diagram, we can see that austenite formation is considered to occur in two steps: firstly the pearlite dissolution and then the transformation of ferrite. For the first step, the nucleation of austenite occurs instantaneously (above temperature AC_1) so that no incubation period is considered. The diffusion distances are short and the transformation is rapid. For the second step the growth of austenite into the ferrite regions is slower: it is controlled by carbon diffusion. At temperature between AC_1 and AC_3, at completion of the transformation some ferrite remains. The maximum amount of austenite that is formed is calculated from the Fe–C equilibrium diagram. Above temperature AC_3, the completion of the transformation corresponds to a full austenitic structure. At each temperature, the growth of austenite is modelled by two Johnson–Mehl–Avrami laws, one for the dissolution of pearlite and the other for the transformation of ferrite.[18]

2.1.2. Evolution of the Carbon Content in Austenite

During rapid heating austenite is not homogeneous in composition. This inhomogeneity will have an effect on the kinetics of transformation during cooling. Thus it is important to know the carbon content in austenite at the end of the heating process. Analytical and numerical treatments of austenite homogenization from one or two phases have been proposed.[8,19-21] They are based on the solution of the diffusion equation. In the present model, we have chosen to use experimental carbon distributions. From the experimental study on a hypoeutectoïd carbon steel[22,23] an evolution law of the carbon content in austenite originating from the pearlite (γ_P) and ferrite (γ_F) regions as a function of the temperature difference $\Delta T=T_{aus}-AC_1$ has been obtained (T_{aus} is the austenitization temperature; AC_1, the beginning temperature of the transformation is here heating rate dependent). This law is described more in

details in Sec. 3.1.

2.1.3. Calculation of Austenite Grain Growth

Several authors[24-26] have studied the effect of time and temperature on the grain growth of austenite during rapid heating. According to the rule of additivity (thermal cycle divided into isothermal time steps), austenite grain growth is described by the following relationship[26]:

$$G^a - G_o^a = k_o \sum_i \Delta t_i \exp\left(-\frac{Q}{RT_i}\right) \quad \text{.....(1)}$$

where G is the austenite grain size during heating, G_o the austenite grain size at the beginning of full austenitization, Δt_i length of time step i, T_i temperature of step i. a, k_o, Q are constants and R is the gas constant.

With these different concepts we get the flowchart of the phase transformation calculation model during heating given on **Fig. 3**.

2.2. Cooling

This model has been put together with the existing model for the calculation of transformations during continuous cooling based on a rule of additivity. We give here only the principal features of the model.[1,2]

Incubation and growth periods are treated separately for diffusion-controlled transformations. The incubation period is determined according to Scheil's method: the transformation during continuous cooling begins when the sum $\sum_i(\Delta t_i/\tau(T_i))$ becomes equal to unity (Δt_i is the length of time step i and $\tau(T_i)$ is the beginning time for the isothermal transformation at temperature T_i). An heredity factor for nucleation (which corrects Scheil's sum) is introduced in order to take into account non additivity at the transition from pearlite to bainite.

The phase growth is modelled according to the law developed by Johnson–Mehl and Avrami. It applies when the austenite transforms into proeutectoid constituent (ferrite/cementite), pearlite or bainite. For the proeutectoid reaction the value of $y_{\max k}$ is deduced from the equilibrium diagram and from the concept of Hultgren's extrapolation. An incomplete bainitic transformation can also be taken into account in the model. For martensitic transformation the progress of transformation is calculated using the relation established by Koistinen and Marburger.

A hardness calculation is associated with this phase transformation calculation. The final hardness is obtained by accumulating the contributions of the different constituents formed along cooling:

$$HV = \sum_i \left(\sum_k \Delta y_{ki} HV_{ki} \right)$$

HV final hardness at a given point, Δy_{ki} increment of phase k formed at time step i, HV_{ki} microhardness of constituent k formed at temperature T_i.

The flowchart of the phase transformation calculation during cooling is recalled on **Fig. 4**.

2.3. Specific Aspects Related to Rapid Heating

The specific aspects of rapid heating (inhomogeneity of austenite and grain size of austenite) have needed new developments of the existing model for calculating phase

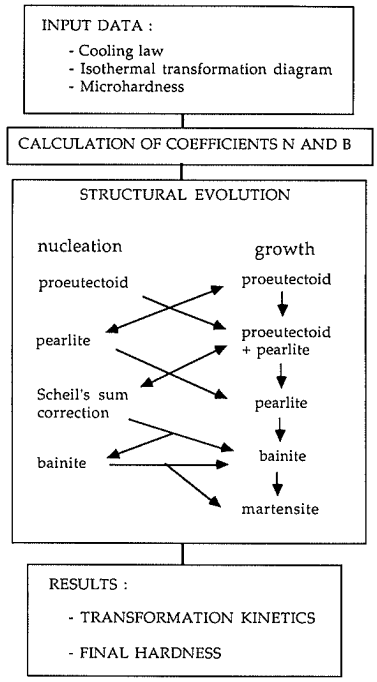

Fig. 4. Flow chart of the phase transformation calculation model on cooling.

transformation during cooling.

2.3.1. Diffusion Dependent Transformations

– The increase of the austenite grain size leads to a slowing down of the transformation. This effect is modelled (for homogeneous austenite) by a shifting in the time scale of the IT cooling diagram. The following set of relations is used in order to describe the effect of grain size on the incubation period as well as on the growth part of the transformation:

$$\tau_g = (1 + D_G)\tau$$

$$n_{kg} = n_k$$

$$b_{kg} = \frac{b_k}{(1 + D_G)^{n_k}}$$

τ_g, n_{kg}, b_{kg} represent the values with effect of grain size.

D_G is a function of the grain size G determined from IT curves for different austenite grain sizes. It is written as a polynomial the coefficients of which are obtained from experimental data.

– When austenite is non homogeneous we consider a spreading out in time of its isothermal transformation kinetics on cooling in comparison with the transformation kinetics of homogeneous austenite. Thus the incubation period of the transformation of the inhomogeneous austenite (τ_D) corresponds to the one of the low carbon austenite γ_F (originating from the ferrite regions).

$$\tau_D = (1 + D_{\gamma_F})\tau$$

D_{γ_F} is a function of ΔC_{γ_F}.

ΔC_{γ_F} is the difference between the carbon content of γ_F and the mean carbon content of the steel.

The new coefficients n_k and b_k of the isothermal kinetics law are determined by using the times t_{1D} and t_{2D} corresponding to 10 and 90% of phase formed:

$$t_{1D}=(1+D_{\gamma F})t_1$$
$$t_{2D}=(1+D_{\gamma P})t_2$$

t_1 and t_2 are the times corresponding to 10 and 90% of phase formed of the original IT diagram of the steel. $D_{\gamma P}$ is a function of $\Delta C_{\gamma P}$. $\Delta C_{\gamma P}$ is the difference between the carbon content of the high carbon austenite γ_P (originating from pearlite) and the mean carbon content of the steel.

$D_{\gamma F}$ and $D_{\gamma P}$ can be obtained from IT curves of steels with different carbon contents. It must be noted that $D_{\gamma F}$ and $D_{\gamma P}$ are respectively negative and positive. As for D_G, they are taken in the form of polynomials.

2.3.2. Martensitic Transformation

– When austenite is inhomogeneous, the model takes into account a variation of Ms tempeature with carbon content. The martensitic start temperatures are respectively $Ms_{\gamma P}$ and $Ms_{\gamma F}$ for the high carbon austenite and for the low carbon austenite:

$$Ms_{\gamma P}=M_{SO}+h\Delta C_{\gamma P}$$
$$Ms_{\gamma F}=M_{SO}+h\Delta C_{\gamma F} \quad \text{.....(2)}$$

M_{SO} is the martensite start temperature for the homogeneous austenite. h is a constant. Thus, the two austenites will have a different progress of martensitic transformation with temperature. In addition, the hardness of martensite is calculated as a function of its carbon content.

– When austenite is homogeneous, Ms temperature is taken as a function of austenite grain size according to our experimental results (Sec. 3.1).

2.4. Coupling with the Thermal Calculation

This phase transformation calculation model has been coupled with the calculation of the temperature distribution in a cylinder during rapid heating and cooling. The temperature distributions are calculated by solving the heat conduction equation. This equation contains a term describing the rate of energy released by the phase transformation. It is related to the enthalpy of the transformation and to the rate of transformation. The thermophysical properties of the material are temperature dependent and related to the volume fractions of phase formed through a linear mixture rule. The details of the thermal calculation model have been given previously.[2,22]

3. Application of the Model

In order to work out the model, an experimental characterization of phase transformations during rapid heating and cooling has been performed on a XC42 carbon steel (study of the kinetics of transformations, microstructural analysis, hardness measurements.[22,23] We present here only the data that will be used for the calculation. Firstly, the model has been applied to dilatometric specimens (without radial temperature gradients). In that case comparisons between the experimental and calculated transformation kinetics and temperature evolutions will be performed. Then we shall illustrate how the model works on cylindrical specimens with high thermal gradients during heating and cooling.

3.1. Input Data

The material used in this study is a XC42 steel with a ferrite pearlite microstructure. The application of the heating part of the model needs the IT heating diagram to be determined either from experiments or taken from literature. In this work, we have chosen a procedure in which the IT diagram is constructed from data obtained during continuous heating on dilatometric specimens. We use a first guess of the IT heating diagram. We then calculate the kinetics of phase transformation during continuous heating. From the comparison with the experimental results, we obtain a new guess of IT diagram. From this iterative scheme the IT heating diagram that can be used for further predictions is determined (Fig. 2).

Figure 5 shows the experimental evolutions of carbon content of the austenite originating either from the pearlite or from the ferrite as a function of the temperature difference between austenitization temperature T_{aus} and AC_1 temperature as it is used in the model. These carbon contents have been measured in the martensitic regions of dilatometric specimens heated up to T_{aus} at different rates and cooled down rapidly.[22] AC_1 depends on the heating rate. When the temperature difference $T_{aus}-AC_1$ is small, the pearlite becomes austenite containing about 0.7% carbon and ferrite becomes austenite with a low carbon conent (~0.02%). When the austenitization conditions increase (temperature, time) carbon diffusion leads to an increase of the carbon content of the low carbon austenite and to a decrease of the carbon content of the high carbon austenite until the mean carbon content of the steel is reached (here for $\Delta T=283$°C).

The coefficients used in the grain growth law (1) are: $a=4$, $k_o=2.969\times10^{15}$ mm^4/mn, $Q=1.269\times10^{15}$ cal/g·atom.[26] We have verified that with these values and an initial grain size $G_o=6\,\mu$m, the law (1) allows to describe well our experimental results that give the austenite grain size *vs.* austenitization temperature for different heating rates (**Fig. 6**).

For the cooling part of the model, we have used an

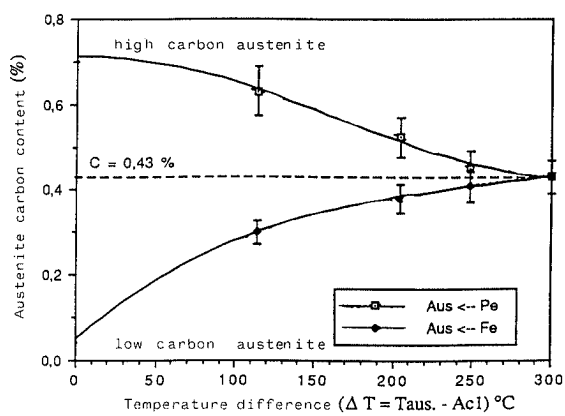

Fig. 5. Variation of carbon content in austenite as a function of heating conditions. The heating rate ranged from 590 to 800°C/s.

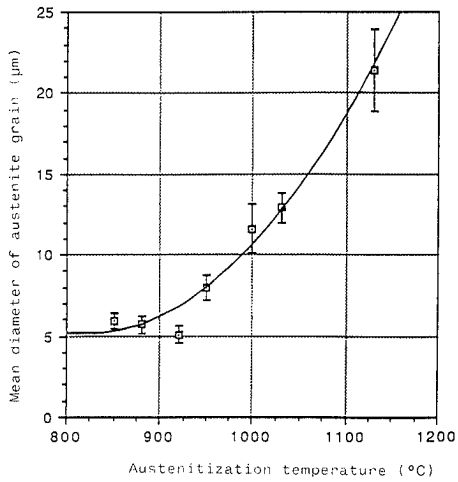

Fig. 6. Variation of austenite grain size *vs.* austenitization temperature. The heating rates ranged from 250 to 710°C/s.

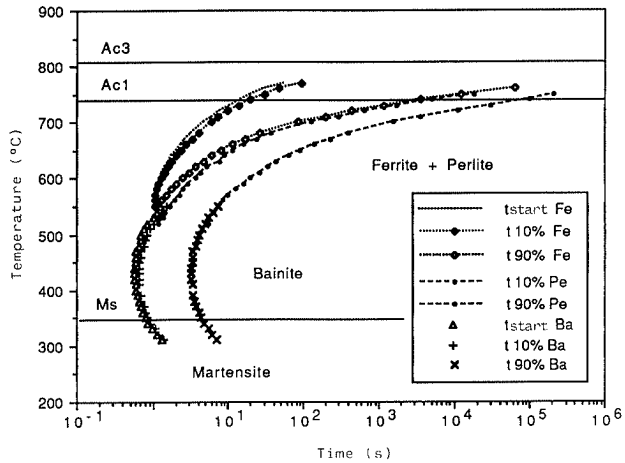

Fig. 7. Isothermal cooling diagram for XC42 steel.

IT cooling diagram from literature and drawn the necessary data for our model (particularly the curves corresponding to 10 and 90% of phase formed that are necessary for the calculation of coefficients n_k and b_k) (**Fig. 7**). For quantifying the effect of the local carbon content of austenite on Ms temperatures we use the law by Andrews[27] that relates Ms temperature to the chemical composition of steels. This law leads to $h=-423$ in Eq. (2).

From our experimental results the evolution of Ms temperature with austenite grain size (**Fig. 8**) has been determined. M_{SO} has been fixed to 310°C. In order to calculate the hardness of martensite as a function of the local carbon content in austenite the experimental evolution law given by Krauss[28] has been used.

The results that will be presented in this paper concern mainly martensitic transformation, therefore we have not taken into account the effect of local carbon content and grain size of austenite on the isothermal kinetics on cooling.

For the calculation of the temperature evolutions, the thermophysical data (thermal conductivity, specific heat, density) as a function of temperature for the austenite and the other constituents have been taken from

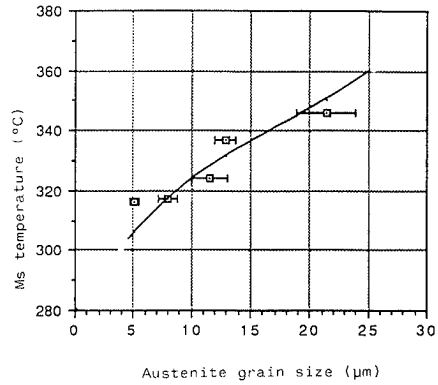

Fig. 8. Ms temperature as function of austenite grain size.

Table 1. Heating and cooling conditions for dilatometric specimens.

Test	Heating rate (°C/s)*	Austenitization temperature (°C)	Cooling rate (°C/s)**
1	60	862	455
2	80	992	395
3	220	982	475
4	600	1 108	470

* Mean rate between 20 and 740°C.
** Mean rate between T_{aus} and 350°C.

literature. The enthalpy of the transformation ferrite+pearlite→austenite has been measured:

$$\Delta H(\mathrm{J/m^3}) = -3.05\times10^8 + 9.26 + 10^3 T + 9.91 T^2 \quad (T:\,^\circ\mathrm{C})$$

For bainitic and martensitic transformation we have used $\Delta H = 4.4\times10^8\,\mathrm{J/m^3}$ and $6.48\times10^8\,\mathrm{J/m^3}$ respectively.[1)]

Moreover the thermal calculation needs the heat flux densities on heating and cooling to be determined. The heat flux densities are obtained using a method of inverse solution of the heat equation[29] in the domains where no transformation occurs. This method uses the experimental temperature evolution at a given point on the radius of the cylinder in order to calculate the surface heat flux densities. In the transformation domains, they are calculated by assuming a linear mixture rule with the volume fractions of the different consituents.[23]

3.2. Application to Dilatometric Specimens

The model has been applied to dilatometric specimens heated at different rates up to different austenitization temperatures and cooled down at a rate greater than the critical cooling rate (**Table 1**).

We present successively the results concerning the temperature evolutions during heating and the martensitic transformation during cooling.

3.2.1. Temperature Evolutions

As an example, **Fig. 9** presents the comparison between the experimental and calculated temperature evolutions during heating and cooling for tests 1 and 4 corresponding to our extreme austenitization conditions.

In both cases a good agreement between experiment

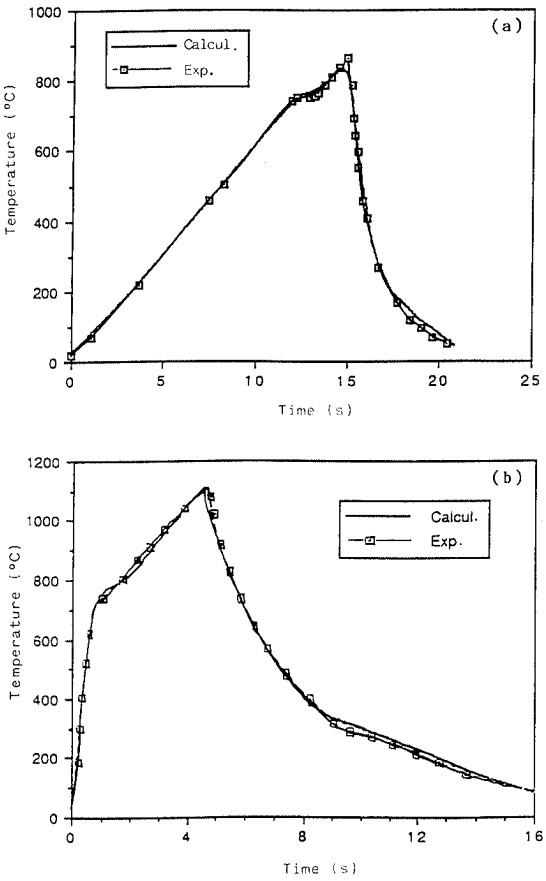

Fig. 9. Comparison between calculated and experimental heating and cooling curves for a dilatometric specimens:
(a) Test 1 (Table 1)
(b) Test 4 (Table 1).

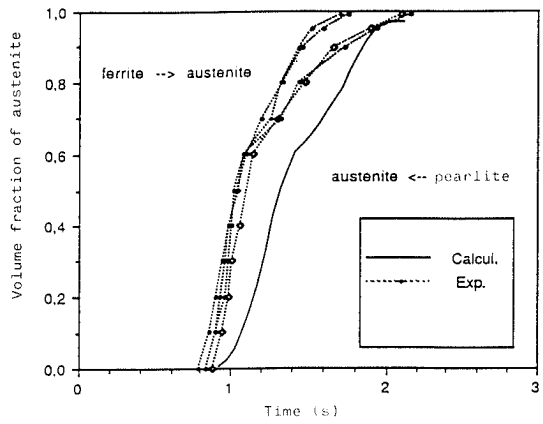

Fig. 10. Comparison between calculated and experimental austenitization kinetics for test 4.

and calculation appears. It must be noted that the specimens are induction heated and the Curie transition leads to a big decrease of the heating rate.

3.2.2. Phase Transformations

– Heating

Figure 10 shows the experimental and calculated austenitization kinetics for test 4. From the experimental point of view, we have reported the results obtained for four tests performed with the same heating conditions. These results illustrate the experimental difficulties to carry out highly reproductible tests at high heating rates.

From the comparison between the calculated result and experiment it comes out that the calculation represents correctly the beginning and the end of the austenitization and the transition from the transformation pearlite → austenite to the transformation ferrite → austenite (at 60% austenite formed). The length of the transformation pearlite → austenite is overestimated by the calculation.

Table 2. Comparison between calculated and measured AC_1 and AC_3 temperatures.

Test	Heating rate	AC_1 (°C)		AC_3 (°C)	
		Exp.	Calc.	Exp.	Calc.
1	60	752	747	820	811
2	80	750	748	821	811
3	220	756	752	828	825
4	600	760	754	838	834

Table 3. Calculated carbon contents in austenite.

Test	Carbon content in austenite (%)	
	γ_P	γ_F
1	0.623	0.299
3	0.467	0.398
2	0.454	0.406
4	0.43	

Table 4. Comparison between calculated and measured austenite grain size.

Test	Grain size (μm)	
	Calc.	Exp.
3	7.0	9.5
2	7.3	10.5
4	18.3	19.0

Table 2 gives a comparison between experimental and calculated beginning temperatures (AC_1) and end temperatures (AC_3) of the transformation. They correspond respectively to 5 and 95% of austenite formed. The agreement is satisfactory. The calculated carbon contents of the low and high carbon austenites are reported in **Table 3**. In that case we have no experimental results to be compared with but the comparison will be carried out in the following in relation with the progress of martensitic transformation that depends on carbon content.

The variations of the austenite grain size for the different austenitization conditions (**Table 4**) are well described by the model if we consider the experimental error (between 0.5 and 2.5 μm).

– Cooling

During cooling the progress of martensitic transformation is calculated. We present here the evolution of the volume fraction of martensite *vs.* temperature

– for tests 1 and 3 where the two austenites with different carbon contents will lead to two different progress of tranformation (**Fig. 11**).

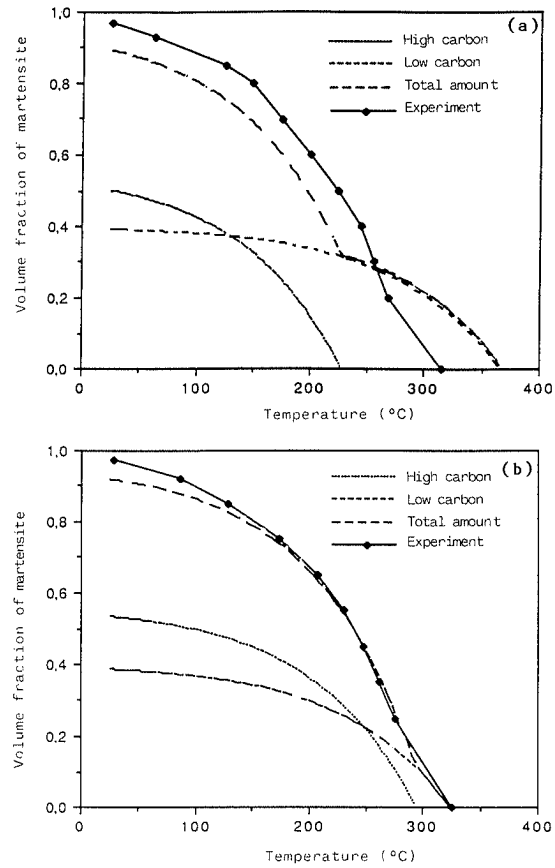

Fig. 11. Progress of martensitic transformation during cooling. Calculated and experimental results for (a) Test 1, (b) Test 3.

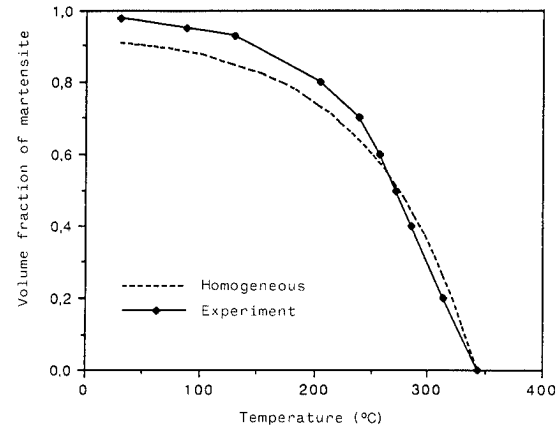

Fig. 12. Progress of martensitic transformation during cooling. Calculated and experimental results for test 4.

– for test 4 where austenite is homogeneous and the austenitic grain size affects the progress of the transformation (**Fig. 12**).

The measured volume fractions of martensite are also reported on these figures. A reasonable agreement between the calculated results and the experiments is obtained in the case of tests 3 and 4 but the final amount of martensite is underestimated by the model. For test 1 the agreement is not good: the calculated martensite start temperature is much higher than the experimental one. This discrepancy can be related to the way of taking into account the inhomogeneity of austenite in the model. Indeed, the experimental carbon evolutions given on Fig. 5 have been obtained for heating rates ranging from 600 to 800°C/s. For much lower heating rates (as for test 1 for which the heating rate is 60°C/s) these data lead to an overestimation of the inhomogeneity of austenite and consequently to a difference between the Ms temperature of the two austenites that is too high. This fact is sustained by the hardness values given in **Table 5**. In the case of test 1 the calculated hardness of the high and low carbon martensites are respectively higher and lower than the measured ones.

For the other tests the experimental and calculated hardnesses show a very reasonable agreement. The difference between the hardness of martensite and the hardness of the specimen calculated for test 4 is due to the retained austenite of the final microstructure. From these results on dilatometric specimens it appears that our model, with the different concepts taken into account, correctly represents the state of austenite at the end of the heating and the following martensitic transformation during cooling.

3.3. Application to Massive Cylinders

3.3.1. Numerical Simulation of a Surface Heat Treatment

We have carried out a numerical simulation of the rapid heating and cooling of a cylinder with 16 mm in diameter. A constant heat flux density is imposed at the surface for heating and for cooling.

Figure 13 shows the temperature evolutions at different locations on the radius of the cylinder. The maximum temperature that is reached at the surface is 1 100°C. This temperature lies below AC_1 temperature (AC_1 ~755°C) in an area between $r=0$ and $r=3.5$ mm.

In order to analyse the state of the austenitization

Table 5. Calculated and measured hardnesses for dilatometric specimens.

Test	Carbon content in austenite (%)		Calculation			Experiment		
			Hardness martensite (HV)		Hardness specimen (HV)	Micro-hardness martensite ($HV_{0.3}$)		Hardness specimen (HV_{10})
	γ_P	γ_F	High carbon	Low carbon		High carbon	Low carbon	
1	0.623	0.299	884	656	749	827	717	745
3	0.467	0.398	806	754	754	809	744	736
2	0.454	0.406	797	761	753	807	752	725
4	0.43		780		748	746		735

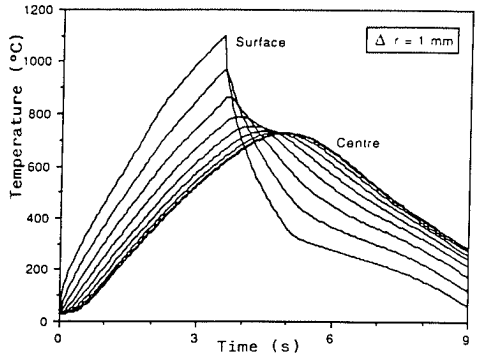

Fig. 13. Temperature evolutions at different locations on the radius of a 16 mm diameter cylinder.

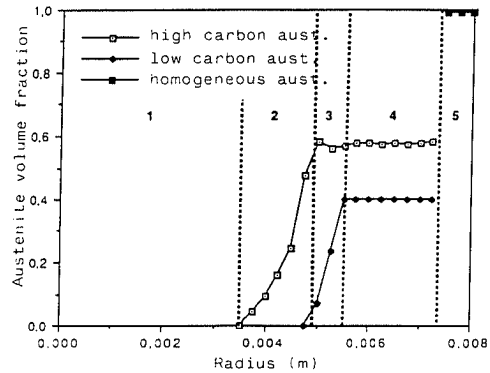

Fig. 14. Volume fraction of austenite along the radius of the cylinder.

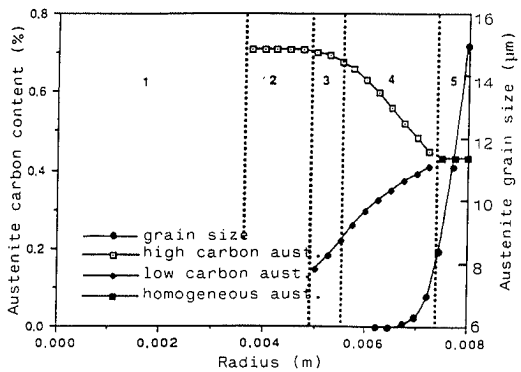

Fig. 15. Carbon content and grain size of austenite along the radius of the cylinder.

along the radius of the cylinder, we show the volume fraction of austenite in **Fig. 14**, the carbon content and the grain size of austenite in **Fig. 15**.

Five zones can be distinguished along the radius:

1: no transformation during heating
2: only the pearlite is transformed into austenite with a high carbon content
3: all the pearlite is transformed (about 60% high carbon austenite exists) and the ferrite becomes austenite with a low carbon content
4: the austenitization process has reached completion and the homogeneization of austenite occurs;
5: austenite is homogeneous and the grain size increases from 6 to 15 μm at the surface.

Of course, these different austenitization states will lead to different transformation kinetics during cooling. **Figure 16** shows the radial distribution of microstructures at the end of cooling.

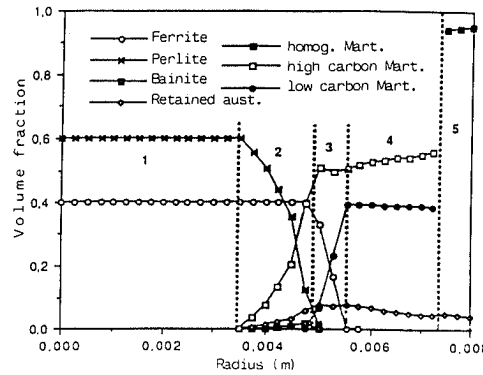

Fig. 16. Radial distribution of microstructures at the end of cooling.

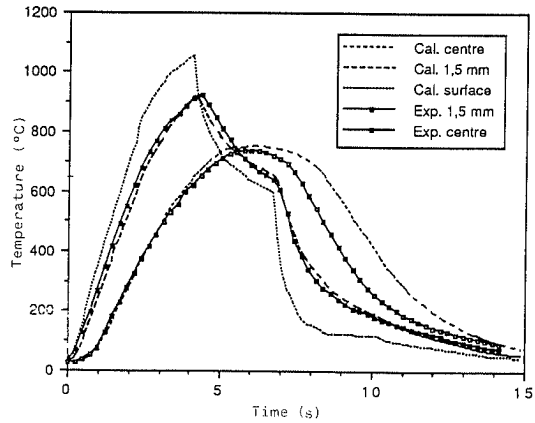

Fig. 17. Comparison between experimental and calculated temperature evolutions during induction hardening of a cylinder 16 mm in diameter.

As expected, in zone 1 we find the original microstructure (60% pearlite, 40% ferrite). In zone 2, the volume fraction of high carbon martensite increases at the expense of pearlite. As a consequence of the low Ms temperature (Ms ~ 180°C) an amount of retained austenite is obtained. There remains 40% ferrite. In zone 3, the amount of high carbon martensite remains nearly constant and the amount of low carbon martensite increases. Zone 4 is made of a mixture of high and low carbon martensites. The amount of high carbon martensite increases slightly and the amount of low carbon martensite decreases slightly. These evolutions are to be related to the variations in Ms temperatures with carbon content. Near the surface (zone 5), the amount of homogeneous martensite reaches 95%. There is 5% retained austenite. These microstructure distributions lead to a radial hardness distribution which is characteristic of a surface hardening treatment. Hardness is high (760 HV) and nearly constant down to a depth of 2 mm and then decreases progressively until the original hardness of the steel (240 HV) is reached at 4.5 mm in depth.

3.2.2. Application to an Induction Treated Cylinder

The calculation model has been applied to a cylinder with 16 mm in diameter (length 48 mm) induction heated and quenched in water at 20°C.

The temperature evolutions are recorded during the treatment by means of two thermocouples located in the center and at a depth of 1.5 mm from the surface in the median plane of the cylinder.

Firstly, the surface heat flux densities have been determined from the measured temperature evolution at 1.5 mm from the surface. Then the model has been applied with the data described previously. The comparison between calculated and measured temperature evolutions is shown in **Fig. 17**. It can be noted that the heating is well described although the thermal calculation does not take into account the eddy current losses due to the electromagnetic field.

As cooling starts at the surface, differences between experiment and calculated results appear. The cooling law in the center is badly described by the calculation. It must be underlined that quenching in vaporisable liquid is a complex case from the point of view of thermal calculations: the different heat transfer stages (film boiling, nucleate boiling convection) may lead to high local thermal gradients, consequently the temperature measurements at one point does not necessarily represent the cooling of the specimen.

Figure 18 shows the measured and calculated radial distributions of hardness. It appears that the calculation describes correctly the evolution of hardness except in the center where the calculated values are above the measured one. This difference is easily explained if we refer to the distributions of microstructure. Experimentally, the original ferrite–pearlite microstructure is kept in the center of the cylinder[23] whereas the calculation gives a microstructure made of ferrite (40%), bainite (15%), martensite (5%) at this point.

This difference is attributed to the discrepancy between calculated and measured temperatures: in the centre, from the measurements it appears that the maximum temperature reached on heating is lower than AC_1 and no transformation has occurred, whereas the calculated maximum temperature is 755°C and 20% austenite has been formed. It must be noticed that the experiment used here is a difficult case from the point of view of comparisons between calculated and experimental results: as the maximum temperature in the center is close to AC_1, a relatively small discrepancy between measured and calculated maximum temperatures leads to big discrepancies between calculated and experimental microstructures. Generally during surface hardening treatments of workpieces, the thermal gradients are much higher than in our experiment.

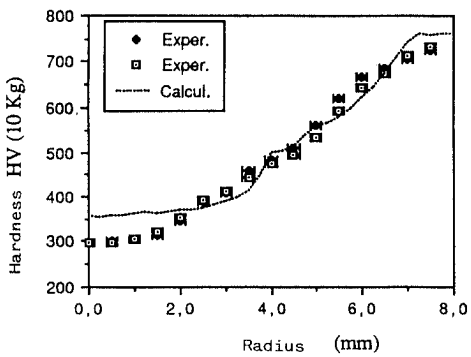

Fig. 18. Measured and calculated hardness profiles after an induction hardening treatment.

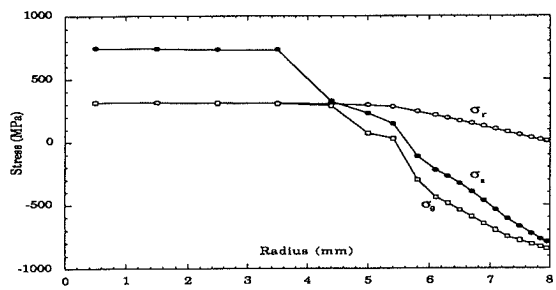

Fig. 19. Calculated radial residual stress profiles after fast heating and cooling of a cylinder 16 mm in diameter.

In addition to the thermal and metallurgical calculations the internal stress analysis during fast heating and cooling of cylinders is now performed. The description of the mechanical constitutive model can be found elsewhere.[30] In this paper we show only as an example the calculated residual stress profiles for the cylinder considered in Sec. 3.2.1.

4. Conclusion

We have developed a model for calculating phase transformations during rapid heating and cooling in steels. The concepts that are taken into account allow to describe in a realistic way the kinetics of austenitization, the state of austenite at the end of heating (carbon content, grain size) and the subsequent transformation during cooling for dilatometric specimens.

The application of the model to a cylindrical specimen heated up with high thermal gradients shows that a thorough description of the state of austenitization and of the final microstructures along the radius is obtained.

In the case of induction hardening the model leads to satisfactory results as regards the predicted final microstructure and hardness distributions (if however the temperature distributions during the treatment can be predicted accurately).

In addition to the prediction of thermal and microstructural evolutions in cylindrical specimens, the internal stress evolutions are also calculated. The complete validation of the modelling by comparing computed results and experiment is on course.

At present, the phase transformation calculation model is also associated with a 2D–3D thermal, mechanical computer code in order to predict microstructure, hardness, residual stresses in workpieces during surface heat treatments (induction hardening, laser hardening). This coupled thermal, metallurgical, mechanical model will be a valuable guide for controlling and optimizing heat treatments.

REFERENCES

1) F. Fernandes: Thèse de Doctorat de l'Institut National Polyetechnique de Lorraine, Nancy, (1985).
2) F. Fernandes, S. Denis and A. Simon: *Mèm. Étud. Sci. Rev. Métall.*, **83** (1986), 355.
3) J. Guisti: Thèse de Doctorat ès Sciences Physiques, Université Pierre et Marie Curie, Paris, (1981).

4) J. B. Leblond and J. Devaux: *Acta Metall.*, **32** (1984), 137.
5) M. Melander: A computational and experimental investigation of induction and laser hardening. Dissertation N° 124, Linköping University, Sweden, (1985).
6) M. Umemoto, N. Komatsubara and I. Tamura: *Tetsu-to-Hagané*, **66** (1980), 400.
7) J. S. Kirkaldy and D. Vernugopalan: Prediction of microstructure and hardenability in low alloy steel, TMS AIME Meeting, Chicago, (1983).
8) H. U. Fritsch and H. W. Bergmann: Influence of the carbon diffusion during laser transformation hardening, Numerical simulation and experimental verification, European Scientific Laser Workshop on Mathematical Simulation, organized by H. W. Bergmann, Lisabon 1989, Sprechsaal Publishing Group-D 8630 COBURG, 31, (1989), 89.
9) B. Hildenwall: Prediction of the residual stresses created during quenching especially the quench response in carburized steels. Dissertation n°39, Linköping University, Sweden, (1979).
10) W. A. Johnson and R. F. Mehl: *Trans. AIME*, **135** (1939), 416.
11) M. Avrami: Kinetics of phase change, Part I: General Theory. J. Chem. Phys. 1939, 7, 1103. Part II: Transformation time relations for random distribution of nucleï, *J. Chem. Phys.*, **8** (1940), 212, part III: Granulation, phase change and microstructure, *J. Chem. Phys.*, **9** (1941), 177.
12) G. R. Speich and A. Szirmae: *Trans. AIME*, **245** (1969), 1063.
13) B. Karlsson: *Z. Metalkd.*, **63** (1972), 160.
14) A. P. Surovtsev and V. V. Yarovoi: *Met. Sci. Heat Treat.*, **9** (1984), 649.
15) A. P. Surovtsev, V. V. Yarovoi, V. E. Sukhanov and A. J. Proklova: *Met. Sci. Heat Treat.*, **2** (1986), 104.
16) V. M. Zalkin: *Met. Sci. Heat Treat.*, **1-2** (1986), 96.
17) G. R. Speich, G. A. Demarest and R. L. Miller: *Metall. Trans.*, **12A** (1981), 1419.
18) D. Farias, S. Denis and A. Simon: Modélisation des transformations de phases des aciers en cycles thermiques rapides, Proc. Ecole de Printemps CNRS-EPFL "Lasers de puissance et Traitement des matériaux," 27–31 May 1991, (to be published).
19) B. Karlsson and L. E. Larsson: *Mater. Sci. Eng.*, **20** (1975), 165.
20) M. G. Ashby and K. E. Easterling: *Acta Metall.*, **32** (1984), 1935.
21) W. Li: Laser transformation hardening of steel surfaces, Doctorat Thesis, University of Luleä, Sweden, (1984).
22) D. Farias, S. Denis and A. Simon: *Trait. Thermi.*, **237** (1990), 63.
23) D. Farias: Traintement thermique laser de l'acier XC42 et modélisation des transformations de phases en cycles thermiques rapides au chauffage et au refroidissement, Thèse de Doctorat, I.N.P.L., Nancy, (1991).
24) J. Wyszkowski: *Iron Steel*, **44** (1970), 77.
25) R. A. Grange: *Metall. Trans.*, **2A** (1971), 65.
26) H. Ikawa, S. Shin, H. Oshige and Y. Mekuchi: *Trans. JWS*, **8** (1977), 46.
27) K. W. Andrews: *J. Iron Steel Inst.*, **203** (1965), No. 7, 721.
28) G. Krauss: Martensitic Transformation, structure and properties in hardenable steels. Hardenability concepts with applications to steel, Proc. AIME, ed. by D. V. Doane and J. S. Kirkaldy, AIME, Warrendale, (1978), 229.
29) A. Azim: Optimisation du refroidissement de trempe d'alliages à base d'aluminium: recherche numérique et caractérisation expérimentale. Thèse de Doctorat, I.N.P.L., Nancy, (1989).
30) S. Denis, S. Sjöström and A. Simon: *Metall. Trans.*, **18A** (1987), 1203.